College Note No. 30

THE COLLEGE OF AERONAUTICS

CRANFIELD

OPTIMUM DESIGN OF A VORTEX TUBE FOR ACHIEVING LARGE TEMPERATURE DROP RATIOS

by

R WESTLEY

NOTE NO. 30
MAY, 1955.

THE COLLEGE OF AERONAUTICS

CRANFIELD

Optimum Design of a Vortex Tube for Achieving Large Temperature Drop Ratios

-by-

R. Westley

SUMMARY

The vortex tube, invented by G.J. Ranque, is a simple device which separates a flow of compressed gas into a hot and a cold stream by means of a high speed vortex. It may have useful applications as a refrigerator and one of the aims of the present investigation was to widen the field of application by increasing the vortex tube's cooling performance.

The tests, described in this report, determined the effect of the hot valve setting, the cold outlet diameter, the inlet nozzle size and the inlet pressure ratios, upon the temperature drop ratio characteristics of a vortex tube.

The results show that, by matching the inlet nozzles and cold outlet diameter to the inlet pressure ratio, it is possible to obtain, over a wide pressure range, a temperature drop which is 0.50 of the isentropic temperature drop.

The optimum cold outlet area is almost independent of the inlet pressure, whilst the optimum inlet area decreases as the pressure ratio increases.

This Note was prepared under Ministry of Supply Contract No. 7/Exptl/565/R3

MEP

CONTENTS

/6.9. ...

CONTENTS (Contd.)

CONTENTS (Contd.)

CONTENTS (Contd.)

/2. Notation ...

2. NOTATION

p_i inlet pressure

p_c cold outlet pressure

p_h hot outlet pressure

Δp_i pressure differential across inlet flow meter

Δp_c " " " cold " "

Δp_h " " " hot " "

T_i inlet temperature

T_c cold "

T_h hot "

$\Delta T_c \equiv (T_i - T_c)$

$\left(\frac{\Delta T_c}{T_i}\right)_1 \equiv \frac{\Delta T_c}{T_i}$ for $\frac{\partial \frac{\Delta T_c}{T_i}}{\partial R} = 0$.

$\left(\frac{\Delta T_c}{T_i}\right)_2 \equiv \frac{\Delta T_c}{T_i}$ for $\frac{\partial \frac{\Delta T_c}{T_i}}{\partial R} = 0, \quad \frac{\partial \left(\frac{\Delta T_c}{T_i}\right)_1}{\partial d_c} = 0$.

$\left(\frac{\Delta T_c}{T_i}\right)_3 \equiv \frac{\Delta T_c}{T_i}$ for $\frac{\partial \frac{\Delta T_c}{T_i}}{\partial R} = 0, \quad \frac{\partial \left(\frac{\Delta T_c}{T_i}\right)_1}{\partial d_c} = 0, \quad \frac{\partial \left(\frac{\Delta T_c}{T_i}\right)_2}{\partial d_i} = 0.$

$\frac{T_c^*}{T_i} \equiv 1 - \left(\frac{\Delta T_c}{T_i}\right)_3$

$1 - \frac{\Delta T_{c\ isentropic}}{T_i} \equiv \left(\frac{p_c}{p_i}\right)^{\frac{\gamma-1}{\gamma}}$ - $\gamma = 1.40$.

$\Delta T_{c2} \equiv \left(\frac{\Delta T_c}{T_i}\right)_2 \times T_i$.

$\Delta T_{c3} \equiv \left(\frac{\Delta T_c}{T_i}\right)_3 \times T_i$.

D diameter of vortex tube

NOTATION (Contd.)

d_c diameter of cold outlet

d_i equivalent inlet nozzle diameter $= \sqrt{\frac{4 \times \text{Total inlet area}}{\pi}}$

l_i length of inlet slot

$\left(\frac{d_c}{D}\right)_1 \equiv \frac{d_c}{D}$ for $\frac{\partial\left(\frac{\Delta T_c}{T_i}\right)}{\partial R} = 0, \quad \frac{\partial\left(\frac{\Delta T_c}{T_i}\right)_1}{\partial \frac{d_c}{D}} = 0$.

$\left(\frac{d_c}{D}\right)_2 \equiv \frac{d_c}{D}$ for $\frac{\partial\left(\frac{\Delta T_c}{T_i}\right)}{\partial R} = 0, \quad \frac{\partial\left(\frac{\Delta T_c}{T_c}\right)_1}{\partial \frac{d_c}{D}} = 0, \quad \frac{\partial\left(\frac{\Delta T_c}{T_i}\right)_2}{\partial \frac{d_i}{D}} = 0.$

$\left(\frac{d_i}{D}\right)_1 \equiv \frac{d_i}{D}$ for $\frac{\partial\left(\frac{\Delta T_c}{T_i}\right)}{\partial R} = 0, \quad \frac{\partial\left(\frac{\Delta T_c}{T_i}\right)_1}{\partial \frac{d_c}{D}} = 0, \quad \frac{\partial\left(\frac{\Delta T_c}{T_i}\right)_2}{\partial \frac{d_i}{D}} = 0.$

R hot valve setting (revolutions)

$\left(\frac{A_c}{A}\right)_2 \equiv \left\{\left(\frac{d_c}{D}\right)_2\right\}^2$

$\left(\frac{A_i}{A}\right)_1 \equiv \left\{\left(\frac{d_i}{D}\right)_1\right\}^2$.

/ 3. Introduction ...

3. INTRODUCTION

The principle of the Ranque or Ranque-Hilsch Vortex Tube is based on the thermal effects associated with a high speed vortex. In its general form the vortex tube separates a flow of compressed gas into two streams, one of which is cold and the other hot. The compressed gas is injected tangentially into a tube to form the vortex. The cold core of the vortex escapes through a diaphragm near the inlet nozzles, whilst the remainder leaves through a restricting valve at the opposite end of the tube.

Simplicity of construction and ease of maintenance, in the absence of moving parts, suggests that the vortex tube might have useful applications as a refrigerator where sources of compressed gas are readily available. At present such applications are limited because the vortex tube has a higher power consumption and the refrigerant is less cold than those of the more complicated refrigerators which are in general use.

The object of this experimental investigation was to determine the effect of various parameters on the vortex tube's cooling performance. In particular, with a view to widening the field of application, it was required to find the optimum design which would supply air at the lowest possible temperature.

The investigation was made on a vortex tube of constant diameter and length, using dry air and the effect on the cold air temperature was determined for combinations of various inlet pressures, inlet nozzle sizes, cold outlet sizes and settings of the hot outlet valve.

The apparatus was designed to investigate additional variables including vortex tube length, cold outlet back pressure and inlet air temperature. The results from these tests will be given in a subsequent report.

4. APPARATUS

4.1. The Vortex Tube

The three main parts of the vortex tube used in these experiments were the inlet chamber, the tube and the hot outlet valve. These are shown in Figures 1 and 2.

4.2. The Inlet Chamber

The inlet chamber consisted of an annular settling chamber which surrounded the inlet nozzle and the cold outlet diaphragm. Compressed air entered the settling chamber and

/was ...

was injected into the tube through 8 inlet nozzles. The cold air passed out through the cold outlet diaphragm whilst the remainder passed along the tube to the hot outlet valve. Arrangements were made in the design of the inlet chamber for changing the inlet nozzle component, the cold outlet diaphragm and the tube length. An exploded view of these components is shown in Figure 3 whilst alternative components are shown in Figure 4. Drawings of the cold outlet diaphragm and inlet nozzle component are shown in Figure 5.

The cold outlet diaphragm was a disc with a central sharp edged orifice and the diameters of the cold outlets of the alternative diaphragms were 1/8 (1/8) 1 inch.

The inlet nozzle component had 8 tangential slots. Each slot had a rectangular cross section and was 1/8in. in depth. Five components were available with slot lengths of 1/8 (1/8) 5/8 inch.

4.3. The Tube

The tube connected the inlet chamber to the hot outlet valve. The internal diameter of the tube was $1\frac{1}{2}$inches. In the present tests the long vortex tube was used, and the distance between the cold diaphragm and the closed hot valve's face was fixed at 65 2/3 tube diameters.

4.4. The Hot Outlet Valve

The proportion of hot to cold air leaving the vortex tube was controlled by an adjustable plug valve at the hot air outlet (Figure 2). The valve consisted of a flat topped conical centre body whose total apex angle was 90°, The smaller base was $1\frac{1}{2}$in. diameter and formed the end of the tube. The valve was moved axially by a screw thread of 20 threads per inch and the position of the valve was shown on a revolution indicator.

4.5. GENERAL APPARATUS

A diagrammatic layout of the vortex tube apparatus is given in Figure 8, general assembly plans in Figures 9 and 10, and a photograph in Figure 7.

4.6. Air Supply

The air compressor was capable of supplying up to 600 cubic feet of free air per minute at a maximum pressure of 100 lb./sq.in. gauge. The compressed air passed through an aftercooler and an activated alumina drier into a reservoir.

/An after ...

An aftercooler bypass allowed the temperature of the air entering the reservoir to be increased when required. The compressed air then passed through the main control valve to a secondary drier and to the vortex tube.

4.7. Hygrometer

A tapping in the inlet pipe to the vortex tube was connected to an Assmann aspirated hygrometer.

4.8. Orifice Flow Meters

Orifice flow meters of British Standard Code design were inserted in the vortex tube's inlet and exit pipes to measure inlet, hot outlet and cold outlet rates of flow.

4.9. Vacuum Supply

Although in the tests described in this report the hot and cold outlet flows from the vortex tube were discharged at atmospheric pressure, the apparatus was also designed to permit the outlet flows to be discharged at below atmospheric pressure. To achieve this the outlet pipes could be switched to tanks which were evacuated by a vacuum pump of 480 cubic ft/min. capacity. The results of these tests will be included in a later note.

4.10. Instrumentation

Mercury and water manometers and dial gauges were used to measure the static pressures in the inlet and outlet pipes of the vortex tube and the pressure differentials across the three flow meters.

The temperatures of the inlet air, cold air and hot air were obtained from thermocouple probes which were inserted into the respective air flows. The probe, whose thermocouple wires were constantin and chromel, is shown in Figure 11. The cold junctions were maintained at $0^{\circ}C$ in an ice bath and the potentials from the thermocouples were fed through a multi selector switch to a balance potentiometer.

The position of the static pressure, differential pressure and temperature measuring points are shown in Figures 9 and 10.

/ 5. ...

5. DETAILS OF TESTS

5.1. Assembly of Vortex Tube

An inlet nozzle component and a cold outlet diaphragm were selected and the vortex tube assembled. The outlet tubes were opened to atmosphere.

5.2. Hot Outlet Valve

The inlet pressure to the vortex tube was kept constant. The hot outlet valve was closed and after an interval of 5-10 minutes the pressure and temperature measurements were recorded. The hot outlet valve was then progressively opened, the inlet pressure kept at the initial value, and the measurements repeated for each position of the hot valve until it was sufficiently opened to give no cold outlet flow. When opened beyond this position atmospheric air was drawn into the vortex tube through the cold diaphragm. The hot valve position for no cold flow could not be accurately located using the cold flow meter. In order to find this position, the cold outlet valve was closed and the internal pressure within the cold outlet tube was brought to atmospheric by adjusting the hot valve.

5.3. Inlet Pressure

The tests were repeated at inlet pressures of $\frac{1}{2}$, 1, 2, 3, 4, 5 and 6 kg/cm.^{2} gauge for various hot valve settings.

5.4. Cold Outlet Diaphragm

The tests were repeated for various sizes of the cold outlet diaphragm between 1/8in. and 1in. retaining the same inlet nozzle component.

5.5. Inlet Nozzles

All the above tests were then repeated for various inlet nozzle components with slot lengths varying between 1/8in. and 5/8in.

The following table summarises the values of the parameters investigated.

Variable	Values tested
Hot valve position	Various, between closed and position of no cold flow
Inlet pressure	$\frac{1}{2}$, 1, 2, 3, 4, 5, 6 kg/cm^2 gauge
Cold outlet diameter	1/8, 1/4, 3/8, $\frac{1}{2}$, 5/8, 3/4, 1 in.
Inlet slot length	1/8, 1/4, 3/8, $\frac{1}{2}$, 5/8 in.

5.6. Humidity

The humidity of the inlet air was recorded during each test. The alumina driers were reactivated to maintain the dew point of the inlet air below -20°C or below the cold air temperature if the latter was itself below -20°C. Considerable scatter was shown on the cold outlet temperature readings when the humidity was not closely controlled.

5.7. Noise

The noise level caused by the operation of the tube was high. This level increased as the inlet pressure increased and as the hot valve was opened.

6. RESULTS

6.1. Definitions and Reduction of Results

The measurements were reduced to non-dimensional forms and are plotted in Figures 12-31.

The non-dimensional parameters used were:-

$\frac{\Delta T_c}{T_i}$, where ΔT_c was the temperature difference between inlet and cold outlet flows and T_i was the absolute inlet temperature;

$\frac{p_i}{p_c}$, where p_i was the inlet pressure and p_c was the cold outlet pressure.

$\frac{d_c}{D}$, where d_c was the cold outlet diameter and D the internal diameter of the vortex tube.

$\frac{d_i}{D}$, where d_i was the diameter of an equivalent circular nozzle whose area equalled the total cross sectional area of the inlet slots.

It was found necessary to investigate the general dependence of the function $\frac{\Delta T_c}{T_i}\left(R, \frac{p_i}{p_c}, \frac{d_c}{D}, \frac{d_i}{D}\right)$ upon its parameters and in particular to determine its behaviour near the points of maximum $\frac{\Delta T_c}{T_i}$.

Let $\left(\frac{\Delta T_c}{T_i}\right)_1$ be defined as the value of $\frac{\Delta T_c}{T_i}$ which satisfies $\frac{\partial \frac{\Delta T_c}{T_i}}{\partial R} = 0$.

Let $\left(\frac{\Delta T_c}{T_i}\right)_2$ be the value of $\frac{\Delta T_c}{T_i}$ which satisfies $\frac{\partial\left(\frac{\Delta T_c}{T_i}\right)_1}{\partial\left(\frac{d_c}{D}\right)} = 0$.

Let $\left(\frac{\Delta T_c}{T_i}\right)_3$ be the value of $\frac{\Delta T_c}{T_i}$ which satisfies $\frac{\partial\left(\frac{\Delta T_c}{T_i}\right)_2}{\partial\left(\frac{d_i}{D}\right)} = 0$.

Let $\left(\frac{d_c}{D}\right)_1$ be the value of $\frac{d_c}{D}$ at $\left(\frac{\Delta T_c}{T_i}\right)_2$

$\left(\frac{d_c}{D}\right)_2$, , , , $\frac{d_c}{D}$ at $\left(\frac{\Delta T_c}{T_i}\right)_3$

$\left(\frac{d_i}{D}\right)_1$, , , , $\frac{d_i}{D}$ at $\left(\frac{\Delta T_c}{T_i}\right)_3$

It will be seen that:-

$$\frac{\Delta T_c}{T_i} = f_1\left(\frac{p_i}{p_c}, \frac{d_i}{D}, \frac{d_c}{D}, R\right) \quad \ldots\ldots\ldots\ldots(1)$$

$$\left(\frac{\Delta T_c}{T_i}\right)_1 = f_2\left(\frac{p_i}{p_c}, \frac{d_i}{D}, \frac{d_c}{D}\right) \quad \ldots\ldots\ldots\ldots(2)$$

$$\left(\frac{\Delta T_c}{T_i}\right)_2 = f_3\left(\frac{p_i}{p_c}, \frac{d_i}{D}\right), \quad \ldots\ldots\ldots\ldots(3)$$

$$\left(\frac{\Delta T_c}{T_i}\right)_3 = f_4\left(\frac{p_i}{p_c}\right). \quad \ldots\ldots\ldots\ldots(4)$$

The function f_1 is obtained direct from the experimental readings, f_2 is obtained graphically from f_1 at the points $\partial f_1/\partial R = 0$,

f_3 " " " " f_2 " " " $\dfrac{\partial f_2}{\partial\left(\frac{d_c}{D}\right)} = 0$,

f_4 " " " " f_3 " " " $\dfrac{\partial f_3}{\partial\left(\frac{d_i}{D}\right)} = 0.$

At each step the number of parameters is reduced by one and the final expression $\left(\Delta T_c/T_i\right)_3$ is the maximum value of $\Delta T_c/T_i$ for any given value of p_i/p_c.

6.2. Variation of cold outlet temperature with valve setting for given inlet nozzles, cold outlet diameters and pressure ratios (Figures 12-18).

The variation of temperature drop ratio is plotted against the valve setting, R, for a typical inlet nozzle of $d_i/D = 0.461$, and for pressure ratios of $p_i/p_c = 1.5, 2, 3, 4, 5,$ and 6. Figures 12-18 give the results for seven different cold outlet diameters.

Similar curves were obtained for inlet nozzles of $\frac{d_i}{D} = .268$, .376, .532, and .595.

$\left(\frac{\Delta T_c}{T_i}\right)_1 = f_1\left(\frac{p_i}{p_c}, \frac{d_c}{D}, \frac{d_i}{D}\right)$ was obtained from maximum points on the curves of $\frac{\Delta T_c}{T_i}$ against R.

/6.3. ...

6.3. Variation of maximum temperature drop with cold outlet diameter (Figures 19-23)

In figures 19-23 the maximum temperature drop $\left(\frac{\Delta T_c}{T_i}\right)_1$, at the optimum valve settings, is plotted against the cold outlet diameter, d_c/D, for each inlet nozzle diameter, and for various inlet pressure ratios. It will be seen for each inlet nozzle that, $\left(\Delta T_c/T_i\right)_1$, has a maximum value, which is denoted by $\left(\Delta T_c/T_i\right)_2$ at the appropriate value of $\frac{d_c}{D}$.

$\left(\frac{\Delta T_c}{T_i}\right)_2 = f_2\left(\frac{p_i}{p_c}, \frac{d_i}{D}\right)$ is plotted against $\frac{d_i}{D}$ in figure 24.

6.4. Variation of maximum temperature drop with inlet nozzle diameter, using optimum hot valve setting, and optimum cold outlet diameter (Figure 24).

Figure 24 shows the variation of $\left(\frac{\Delta T_c}{T_i}\right)_2$, with inlet diameter for various inlet pressure ratios. The maximum value of $\left(\frac{\Delta T_c}{T_i}\right)_2$, denoted by $\left(\frac{\Delta T_c}{T_i}\right)_3$, was found for each value of inlet pressure ratio.

$\left(\frac{\Delta T_c}{T_i}\right)_3$ is plotted against the inlet pressure ratio, $\left(\frac{p_i}{p_c}\right)$, in Figure 25.

6.5. Variation of maximum temperature drop with inlet pressure ratio, using optimum hot valve setting, cold outlet diameter, and inlet nozzle diameter (Figure 25)

Figure 25 shows that, $\left(\frac{\Delta T_c}{T_i}\right)_3$, increases continuously with increase of inlet pressure ratio, $\frac{p_i}{p_c}$, and it is therefore not possible to obtain a further maximum.

/6.6. ...

6.6. Empirical Laws for variation of maximum temperature drop with pressure ratio (Figures 26 and 27)

Figures 26 and 27 indicate that two approximate empirical laws may be used to represent the variation of maximum temperature drop with pressure ratio. In figure 26, T_c^* is the minimum cold temperature, and in figure 27, $\Delta T_{c\ \text{isentropic}}$ was calculated from the isentropic equation:-

$$1 - \frac{\Delta T_{c\ \text{isentropic}}}{T_i} = \left(\frac{p_c}{p_i}\right)^{\frac{\gamma-1}{\gamma}} \quad \text{where } \gamma = 1.4 \text{ for air.}$$

6.7. Variation of optimum cold outlet diameter, with inlet diameter (Figure 28)

Figure 28 shows the optimum cold outlet diameter, $\left(\frac{d_c}{D}\right)_1$ for a given inlet diameter. Values of $\left(\frac{d_c}{D}\right)_1$ are plotted against $\frac{d_i}{D}$ for various inlet pressure ratios.

6.8. Variation of optimum cold outlet diameter with pressure ratio (Figure 29)

In figure 29, $\left(\frac{d_c}{D}\right)_1$ is plotted against $\frac{p_i}{p_c}$ for the five inlet nozzle components.

6.9. Variation of temperature drop efficiency with pressure ratio for optimum cold outlet diameter, and fixed inlet diameters (Figure 30)

The temperature drop efficiency was defined as $\frac{\Delta T_c}{\Delta T_{c\ \text{isentropic}}}$.

Figure 30 indicates the performance which could be obtained from a vortex tube with fixed inlet nozzle, and with a cold outlet diameter adjusted to the optimum value.

6.10. Optimum inlet and cold outlet diameters at maximum temperature drop (Figure 31)

The optimum inlet nozzle diameter, $\left(\frac{d_i}{D}\right)_1$, was obtained from figure 24. It is defined as the value of $\frac{d_i}{D}$ at $\left(\frac{\Delta T_c}{T_i}\right)_3$. The corresponding value of $\frac{d_c}{D}$, denoted by $\left(\frac{d_c}{D}\right)_2$, was obtained

/from the ...

from the curves of $\left(\frac{d_c}{D}\right)_1$ against $\frac{d_i}{D}$ in figure 28.

Figure 31 gives the values of the optimum inlet nozzle diameter, and cold outlet diameter, which will give the largest temperature drop at any given pressure ratio.

6.11. Optimum inlet and cold outlet areas at maximum temperature drop (Figure 32)

The optimum inlet nozzle and cold outlet diameters from figure 31 have been replotted in terms of the nozzle inlet area, A_i, the cold outlet area, A_c, and the tube area A.

7. DISCUSSION OF RESULTS

The results show that the temperature drop ratio, $\frac{\Delta T_c}{T_i}$, is dependent on the hot valve setting, R, the cold outlet diameter d_c, the inlet nozzle diameter, d_i, and the inlet pressure ratio, p_i/p_c. The results have been analysed to determine conditions for the maximum temperature drop.

7.1. Variation of temperature drop ratio with hot valve setting

The variation of temperature drop ratio with hot valve setting is shown in figures 12-18 for a typical inlet nozzle of $\frac{d_i}{D} = .461$. As the hot valve is opened the temperature drop ratio increases to a maximum and then falls to a finite value at the point of no cold flow.

An increase of inlet pressure ratio results in an increase of the temperature drop ratio and the curves are extended in the directions of both the $\Delta T_c/T_i$ and R axes. For small fixed values of R it will be noted that the temperature drop ratio at first increases rapidly with increase of pressure ratio and then levels off to values which do not significantly increase with further increase of pressure ratio. If advantage is to be taken of an increased pressure to produce larger temperature drops then it will be necessary to increase R to a higher value.

Comparison of succeeding figures indicates that the temperature drop characteristics are modified as the cold outlet diameter increases. Increase of cold outlet diameter at first results in a general increase of temperature drop.

/A maximum ...

A maximum is then reached and further increase of cold outlet diameter causes a fall in the temperature drop and the curves are extended along the R axis.

7.2. Variation of maximum temperature ratio with cold outlet diameter

The maximum temperature drop ratio from the $\frac{\Delta T_c}{T_i}$ and R curves, is plotted against the cold outlet diameter in figures 19-23 for each inlet nozzle. The curves are similar and show the optimum cold outlet diameters which give the greatest temperature drop ratios for given pressure ratios and inlet nozzle diameter. For a given inlet nozzle the optimum cold outlet diameter is not greatly dependent on the inlet pressure. Figure 29 shows this variation.

For the smallest inlet nozzle of $\frac{d_i}{D} = .266$ the optimum $\frac{d_c}{D}$ increases from .356 at a pressure ratio of 2 to .385 at a pressure of 7. For the largest inlet nozzle of $\frac{d_i}{D} = .595$, the optimum, $\frac{d_c}{D}$, decreases from .350 at a pressure ratio of 2 to .309 at a pressure ratio of 7.

In figure 28 the optimum cold outlet diameter $\left(\frac{d_c}{D}\right)_1$ is plotted against the inlet diameter for various inlet pressure ratios. Figure 30 shows the variation of temperature drop efficiency $\Delta T_c / \Delta T_{i_{isentropic}}$ against pressure ratio for various inlet diameters.

7.3. Variation of temperature drop ratio with inlet diameter

The maximum values of $\left(\frac{\Delta T_c}{T_i}\right)_2$ from figures 19-23 have been plotted, in figure 24, against inlet diameters. It will be seen that the optimum inlet diameter for maximum temperature drop decreases as the inlet pressure increases. The corresponding value of the optimum cold outlet diameter $(d_c/D)_2$ is obtained from figure 28 and the optimum values of inlet diameter and cold outlet diameter are plotted in figure 31. It is noted in figure 28 that the optimum value $(d_c/D)_2$ occurs near the maximum of the curves of $(d_c/D)_1$ against d_i/D.

/The maximum ...

The maximum temperature ratio obtainable with the best combination of hot valve setting, inlet diameter and cold outlet diameter is plotted against inlet pressure ratio in figure 25. The temperature drop ratio, $(\Delta T_c/T_i)_3$ increases from .09 at $\frac{p_i}{p_c} = 2$, to .167 at $\frac{p_i}{p_c} = 4$, and to .217 at $\frac{p_i}{p_c} = 8$. The rate of increase of the temperature drop ratio falls off as the pressure increases.

It can be shown that the temperature drop ratio may be represented by empirical expressions:-

$$\frac{T_c^*}{T_i} \sim \left(\frac{p_c}{p_i}\right)^{\frac{n-1}{n}}$$

where $n = 1.15$,

and T_c^* = the cold air temperature under optimum conditions,

and by

$$\frac{(\Delta T_c)_3}{\Delta T_{c_{isentropic}}} \sim .507 .$$

The corresponding values of $\left(\frac{d_c}{D}\right)_2$ and $\left(\frac{d_i}{D}\right)_1$ which give this maximum temperature drop may be obtained from figure 31 for any given pressure ratio. A plot of optimum inlet area and optimum outlet area in figure 32 gives the empirical relations:-

$$\left(\frac{A_i}{A}\right)_1 \sim .156 + .176 \frac{p_c}{p_i}$$

and

$$\left(\frac{A_c}{A}\right)_2 \sim .167.$$

Thus a vortex tube, designed to give the maximum temperature drop, will require smaller inlet nozzles as the inlet pressure ratio increases. The optimum cold outlet diameter is almost independent of inlet pressure ratio.

/8. ...

8. ACKNOWLEDGEMENTS

Thanks are due to members of the Department of Aerodynamics and the Engineering Department for the manufacture of the apparatus and to Messrs. Haydon and Salisbury who assisted in the running of the tests and the evaluation of the results.

This investigation was supported by a Ministry of Supply Contract and was conducted under the supervision of Mr. G.M. Lilley.

9. CONCLUSIONS

1. The tests show that the temperature drop characteristics of a vortex tube are dependent on the inlet pressure ratio, the inlet nozzle size, cold outlet diameter and hot valve setting.

2. The temperature of the cold air decreased with increase of pressure and the lowest temperatures were obtained when the hot valve setting, cold outlet diameter and inlet nozzle size were matched to the inlet pressure ratio.

3. By using the optimum values of these variables it was possible to obtain temperature drops which were .50 of the isentropic temperature drop. This efficiency was maintainable up to an inlet pressure ratio of 7.5.

4. The optimum cold outlet size was not greatly dependent upon the inlet pressure ratio and was given by the expression.-

$$\frac{\text{Optimum cold outlet area}}{\text{vortex tube area}} \simeq .167 .$$

The optimum inlet area decreased as the inlet pressure ratio increased and was given by.-

$$\frac{\text{Optimum inlet area}}{\text{vortex area}} \simeq .156 + \frac{.176}{\text{inlet pressure ratio}}$$

---

10. BIBLIOGRAPHY

1. R. Westley — Bibliography and Survey of the Vortex tube. College of Aeronautics Tech. Note No. 9 (1954).

2. G. Ranque — 'Histoire de Vortex Tube', April 1955, (Unpublished).

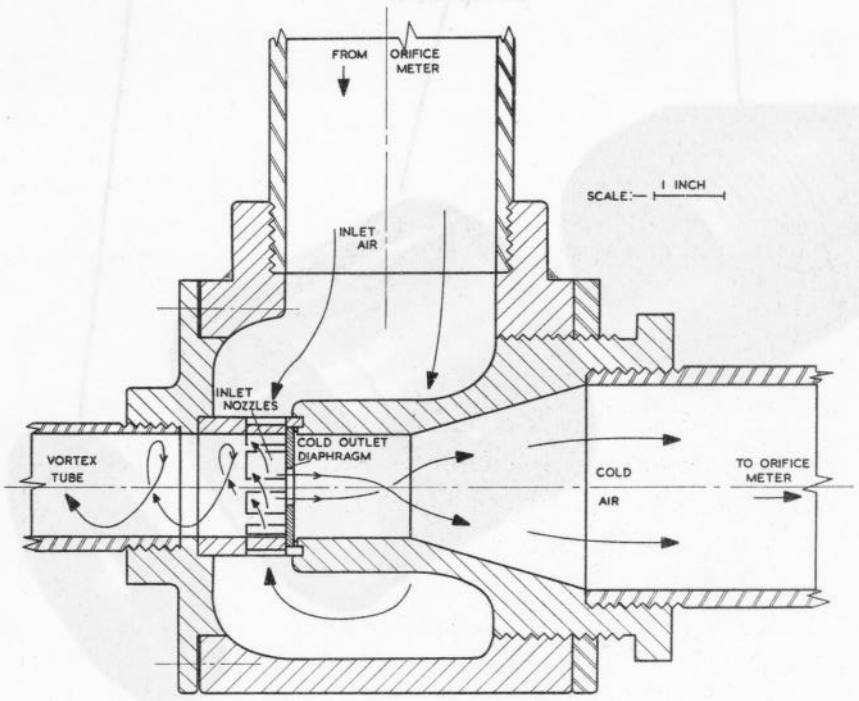

INLET CHAMBER AND COLD OUTLET

FIG. 1.

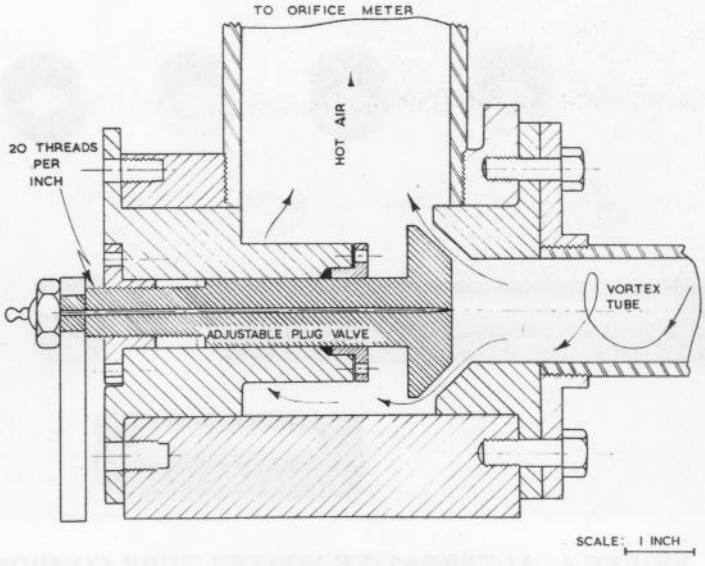

HOT AIR OUTLET VALVE

FIG. 2.

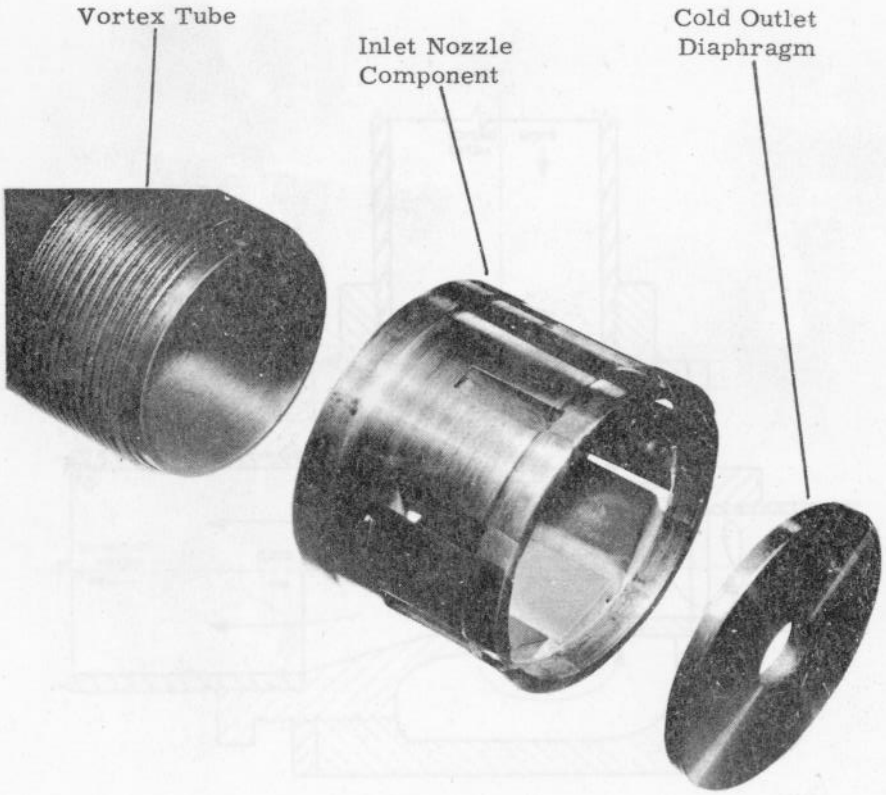

FIGURE 3. EXPLODED VIEW OF COLD OUTLET DIAPHRAGM, INLET NOZZLE COMPONENT AND TUBE.

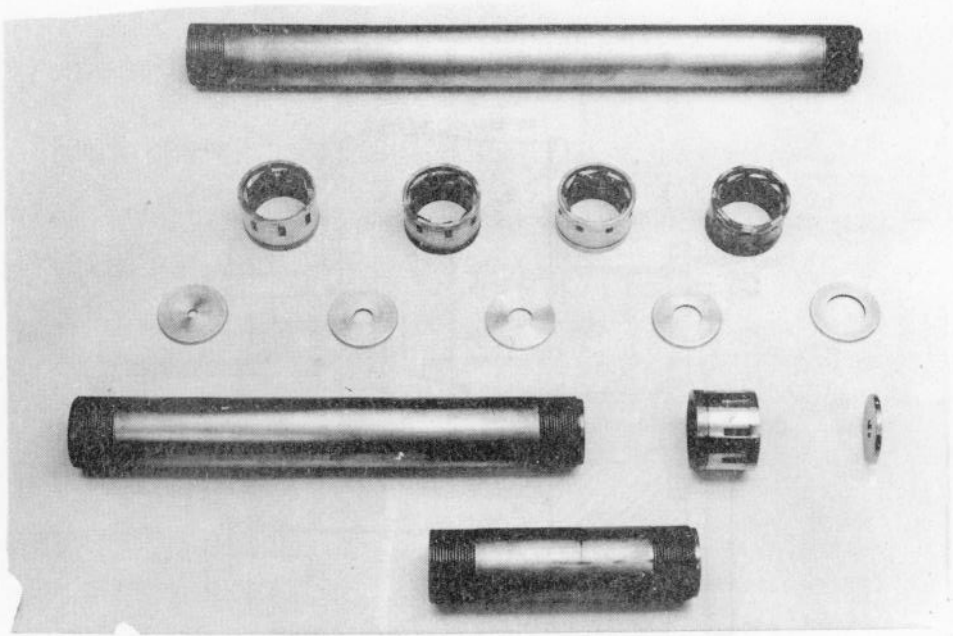

FIGURE 4. ALTERNATIVE VORTEX TUBE COMPONENTS

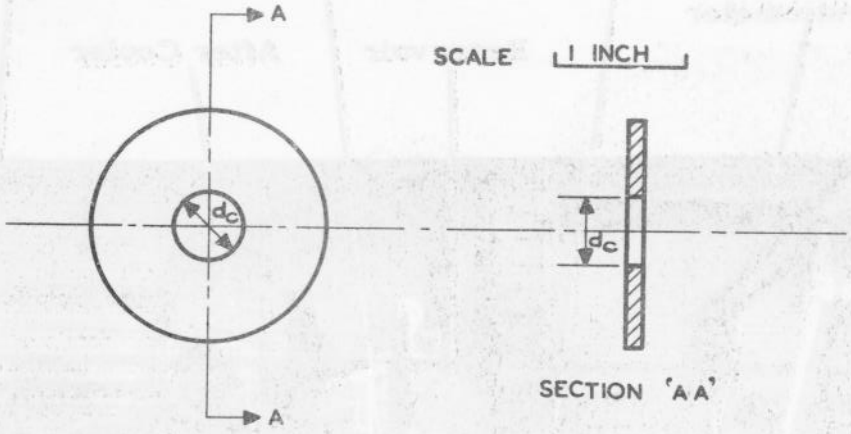

FIGURE 5. COLD OUTLET DIAPHRAGM

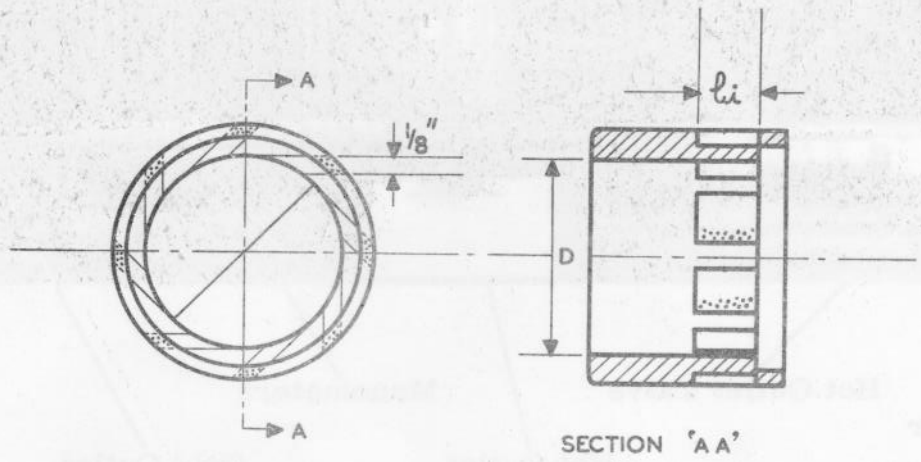

FIGURE 6. INLET NOZZLES

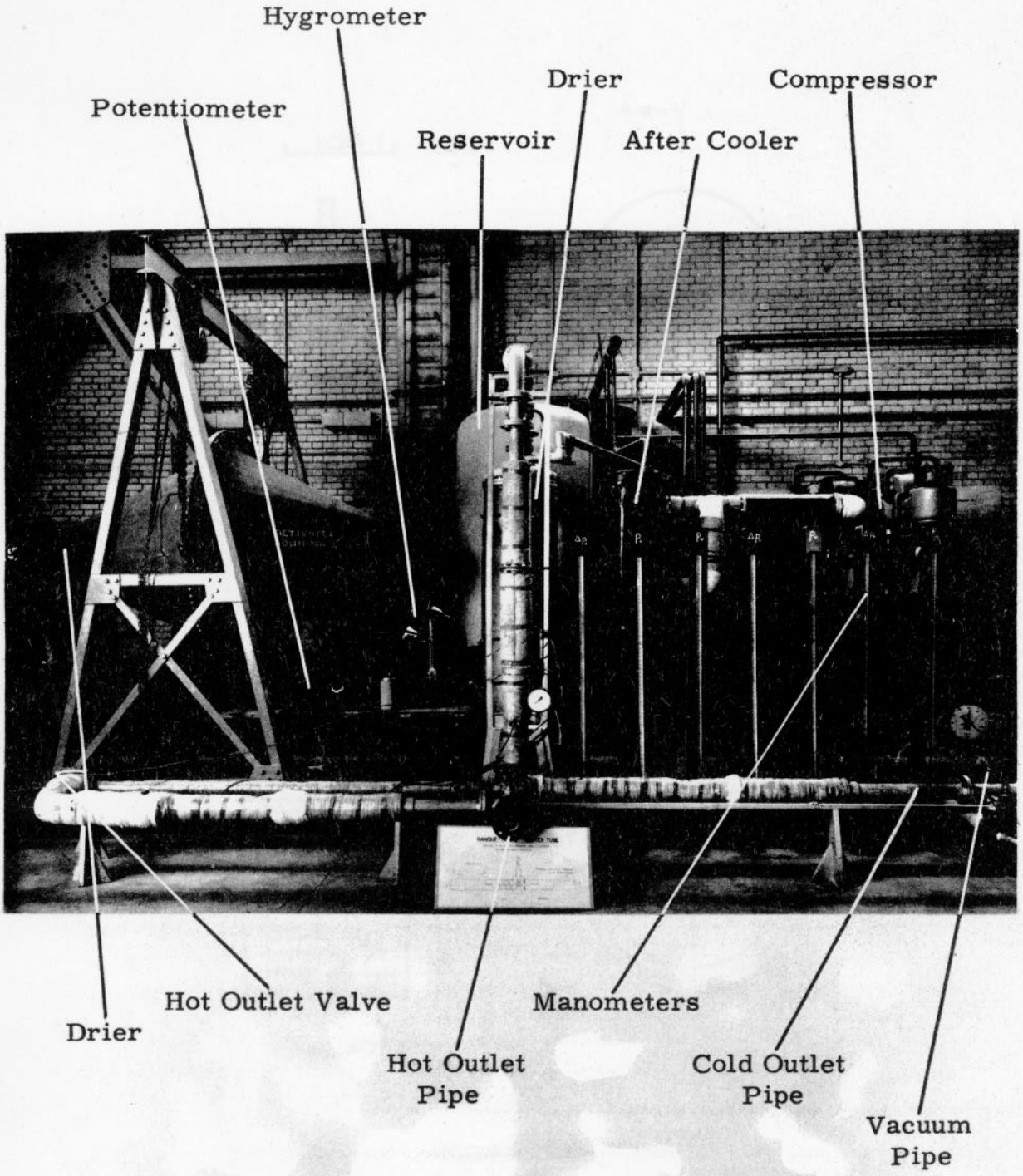

FIGURE 7. GENERAL VIEW OF VORTEX TUBE APPARATUS

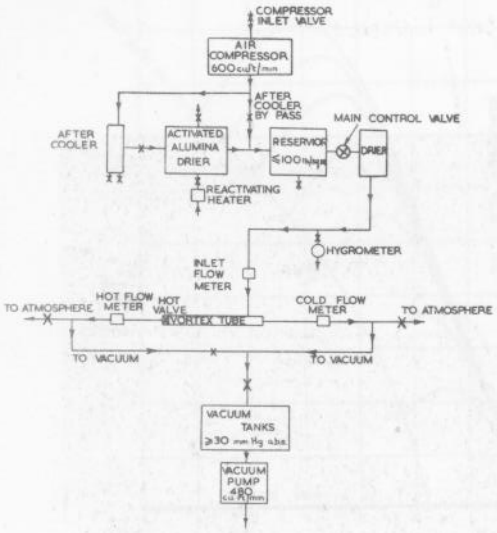

GENERAL LAYOUT OF VORTEX TUBE APPARATUS

FIG. 8.

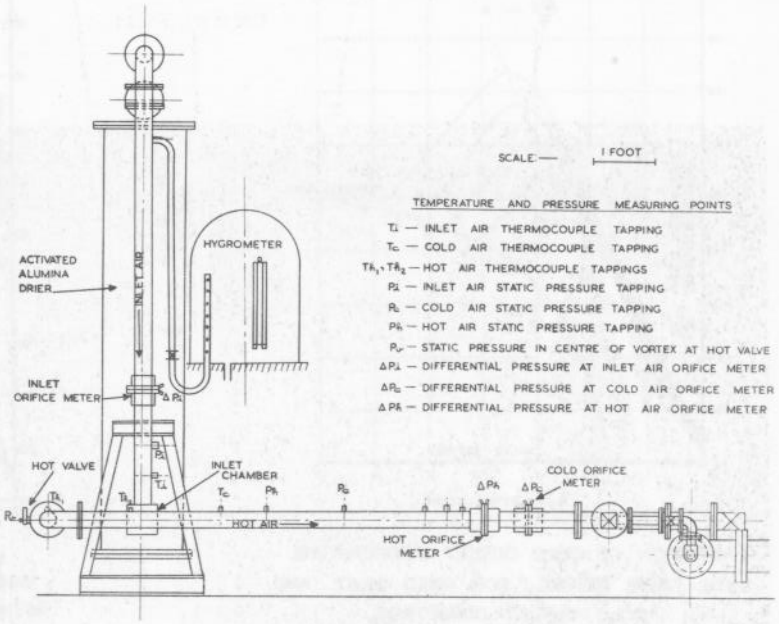

VORTEX TUBE APPARATUS GENERAL ASSEMBLY FRONT VIEW.

FIG. 9

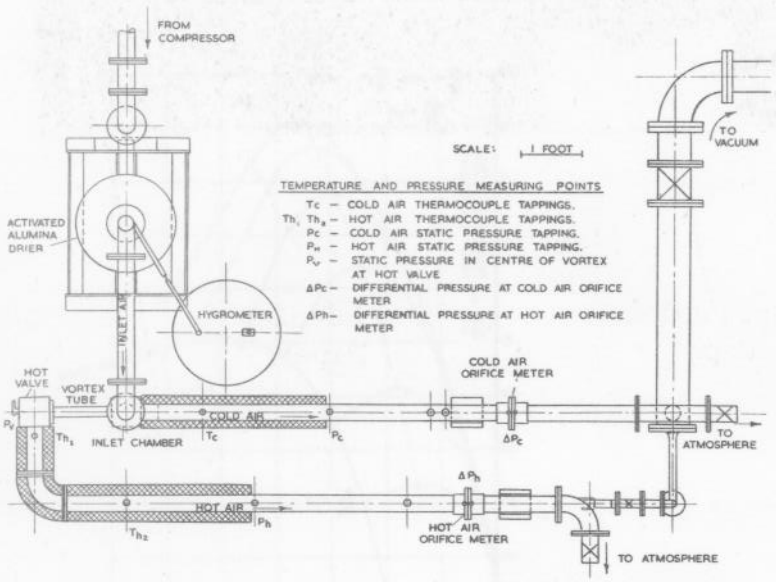

VORTEX TUBE APPARATUS GENERAL ASSEMBLY PLAN VIEW.

FIG. 10.

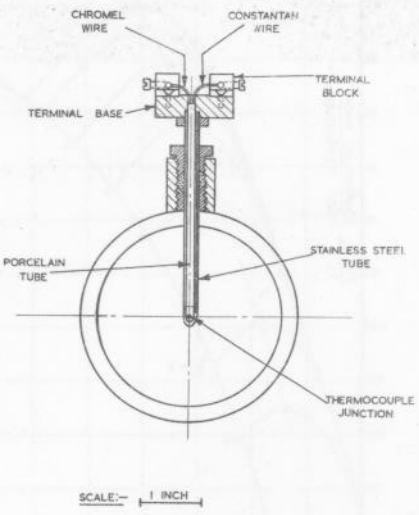

THERMOCOUPLE PROBE.

FIG. 11.

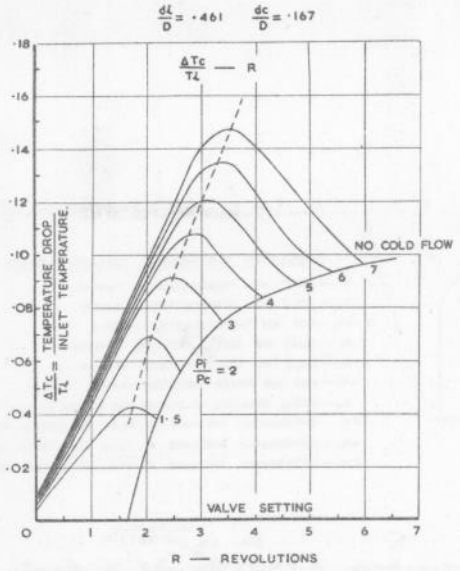

VARIATION OF COLD OUTLET TEMPERATURE WITH VALVE SETTING FOR FIXED INLET AND COLD OUTLET DIAMETERS.

FIG. 12.

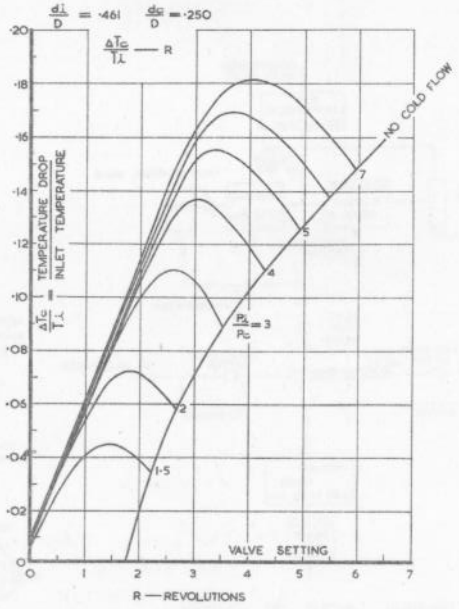

VARIATION OF COLD OUTLET TEMPERATURE WITH VALVE SETTING FOR FIXED INLET AND COLD OUTLET DIAMETERS.

FIG. 13.

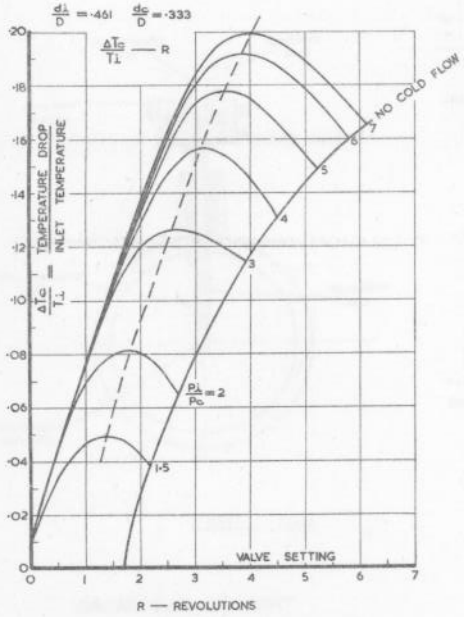

VARIATION OF COLD OUTLET TEMPERATURE WITH VALVE SETTING FOR FIXED INLET AND COLD OUTLET DIAMETERS.

FIG. 14.

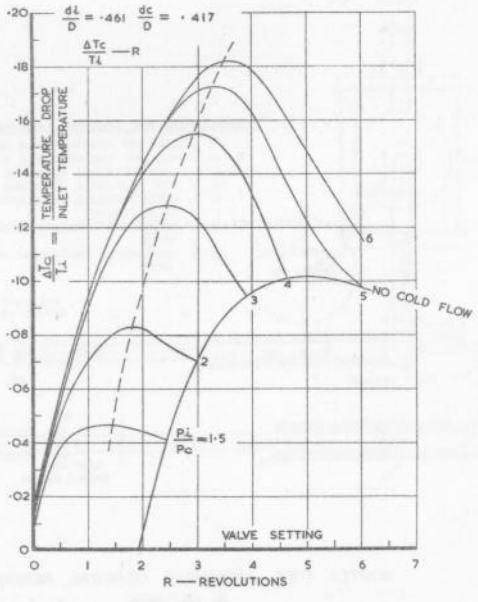

VARIATION OF COLD OUTLET TEMPERATURE WITH VALVE SETTING FOR FIXED INLET AND COLD OUTLET DIAMETERS.

FIG. 15.

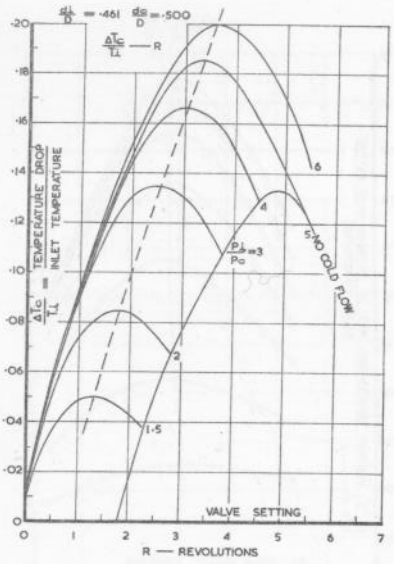

VARIATION OF COLD OUTLET TEMPERATURE WITH VALVE SETTING FOR FIXED INLET AND COLD OUTLET DIAMETERS.

FIG. 16.

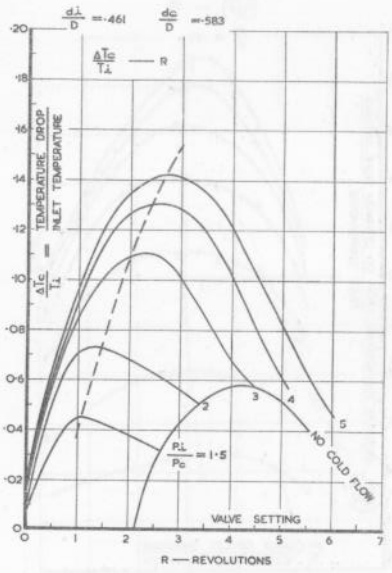

VARIATION OF COLD OUTLET TEMPERATURE WITH VALVE SETTING FOR FIXED INLET AND COLD OUTLET DIAMETERS.

FIG. 17.

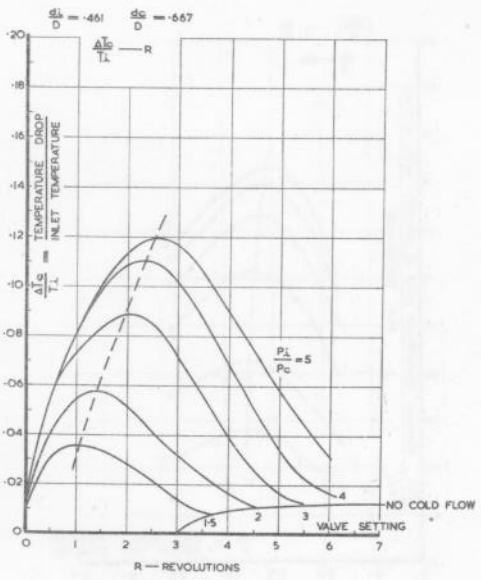

VARIATION OF COLD OUTLET TEMPERATURE WITH VALVE SETTING FOR FIXED INLET AND COLD OUTLET DIAMETERS.

FIG. 18.

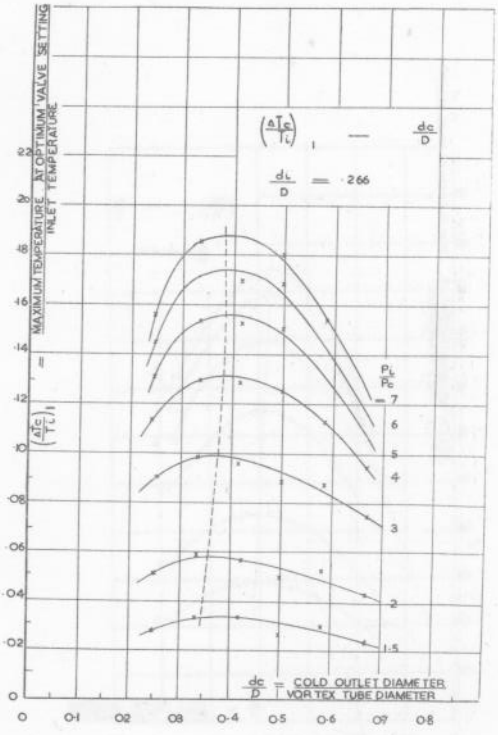

VARIATION OF MAXIMUM TEMPERATURE DROP WITH COLD OUTLET DIAMETER.

FIG. 19.

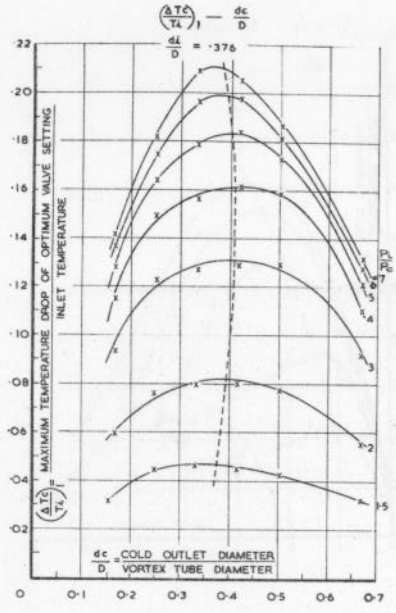

VARIATION OF MAXIMUM TEMPERATURE DROP WITH COLD OUTLET DIAMETER.

FIG. 20.

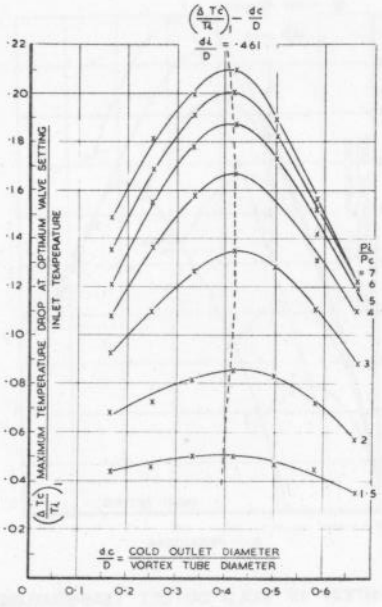

VARIATION OF MAXIMUM TEMPERATURE DROP WITH COLD OUTLET DIAMETER

FIG. 21.

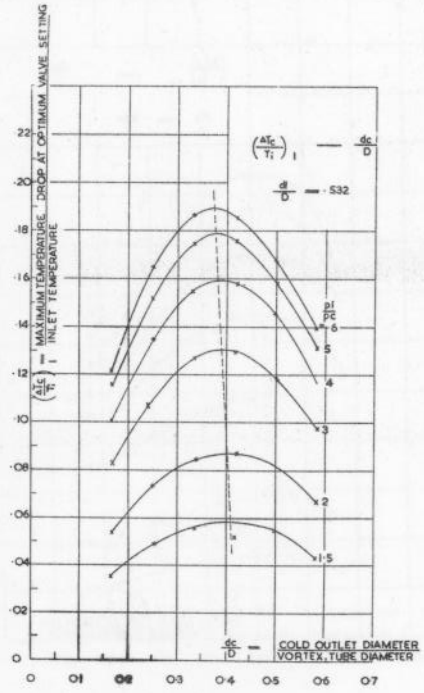

VARIATION OF MAXIMUM TEMPERATURE DROP WITH COLD OUTLET DIAMETER.

FIG. 22.

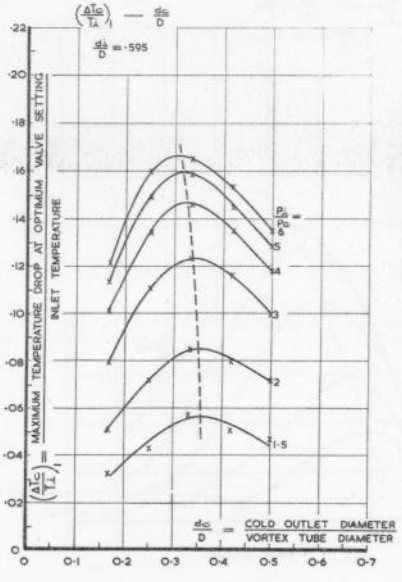

VARIATION OF MAXIMUM TEMPERATURE DROP WITH COLD OUTLET DIAMETER.

FIG. 23.

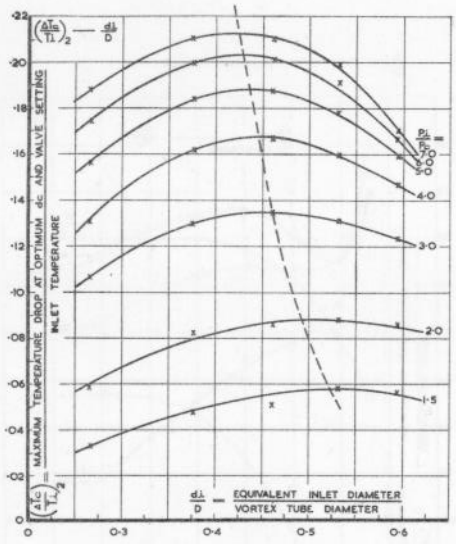

VARIATION OF TEMPERATURE DROP WITH INLET DIAMETER.

FIG. 24.

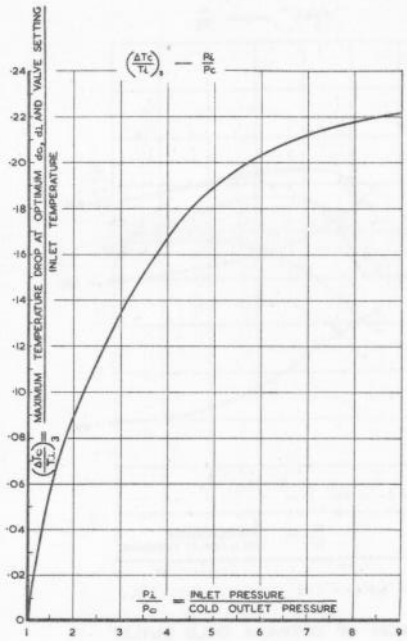

MAXIMUM TEPERATURE DROP FOR OPTIMUM INLET AND COLD OUTLET AREAS.

FIG. 25.

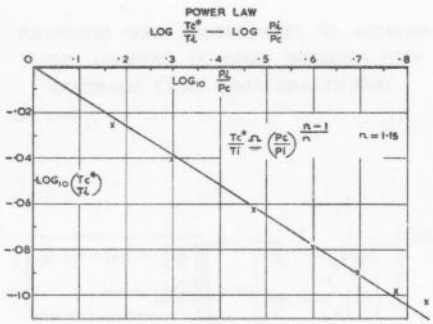

VARIATION OF TEMPERATURE DROP WITH PRESSURE RATIO.

FIG. 26.

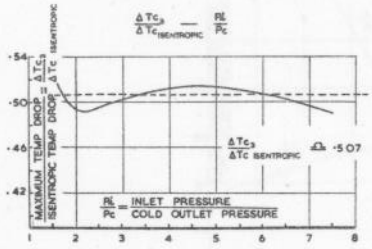

TEMPERATURE DROP AS FRACTION OF ISENTROPIC.

FIG. 27

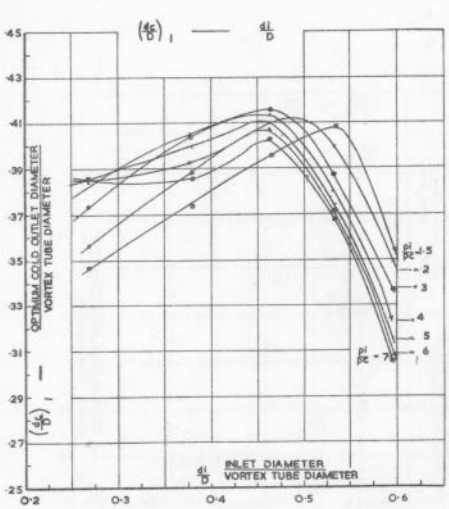

VARIATION OF OPTIMUM COLD OUTLET DIAMETER WITH INLET DIAMETER.

FIG. 28.

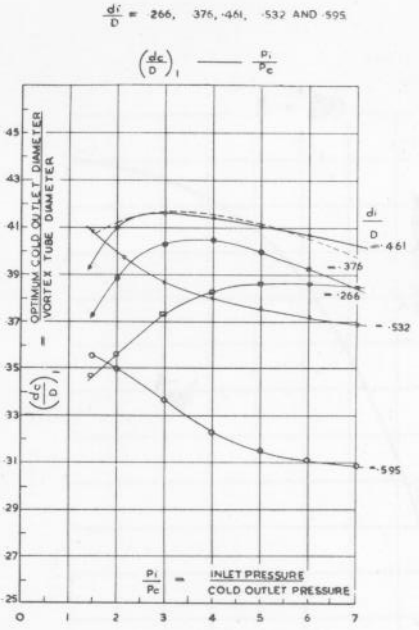

VARIATION OF OPTIMUM COLD OUTLET DIAMETERS WITH PRESSURE RATIO FOR VARIOUS INLET DIAMETERS.

FIG. 29.

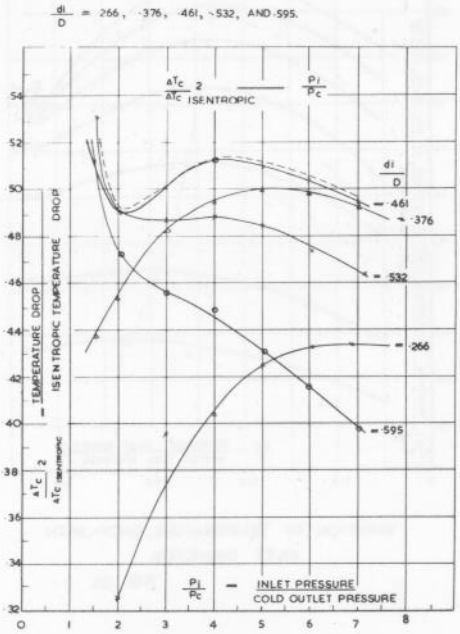

VARIATION OF TEMPERATURE DROP EFFICIENCY WITH PRESSURE RATIO AT OPTIMUM COLD OUTLET AND FIXED INLET DIAMETERS.

FIG. 30.

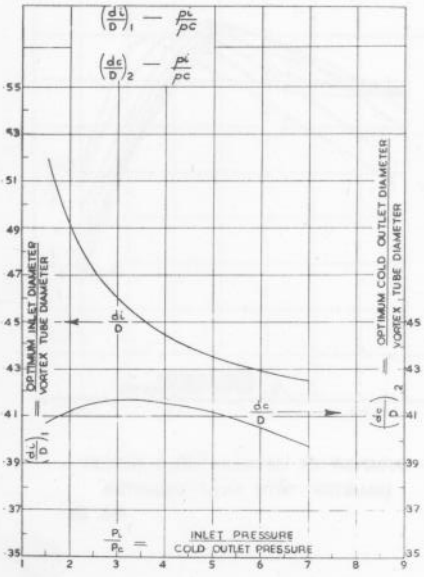

OPTIMUM INLET AND COLD OUTLET DIAMETERS FOR MAXIMUM TEMPERATURE DROP

FIG. 31.

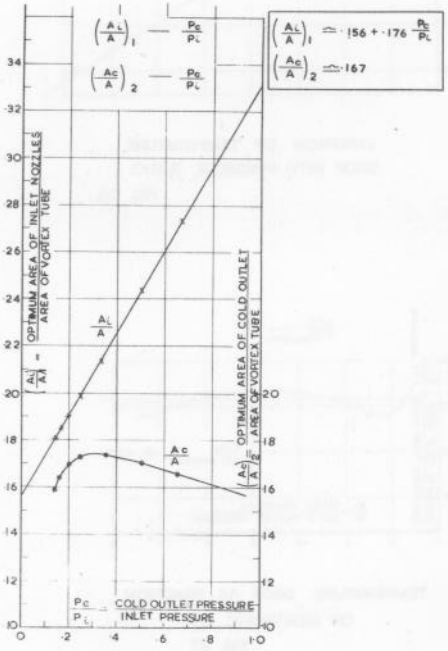

OPTIMUM INLET AND COLD OUTLET AREAS FOR MAXIMUM TEMPERATURE DROP

FIG. 32.